

1 **A model-based investigation of the recent rebound of shelf**
2 **water salinity in the Ross Sea**

3 Jingwei Zhang^{1,2}, Xuebin Zhang¹, Matt A. King^{2,3} and Kewei Lyu⁴

4 ¹Climate Science Centre, CSIRO Environment, Hobart, Australia

5 ²School of Geography, Planning, and Spatial Sciences, University of Tasmania, Hobart,
6 Australia

7 ³The Australian Centre for Excellence in Antarctic Science, University of Tasmania, Hobart,
8 Australia

9 ⁴State Key Laboratory of Marine Environmental Science, College of Ocean and Earth
10 Sciences, Xiamen University, Xiamen, China

11

12

13

14

15

16

17

18

19

20

21

22 **Abstract**

23 Intense atmosphere-ocean-ice interactions in the Ross Sea play a vital role in global
24 overturning circulation by supplying saline and dense shelf waters. Since the 1960s,
25 freshening of the Ross Sea shelf water has led to a decline in Antarctic Bottom Water
26 formation. Since the early 2010s, however, the salinity of the western Ross Sea has
27 rebounded. This study adopts an ocean-sea ice model to investigate the causes of this salinity
28 rebound. Model-based salinity budget analysis indicates that the salinity rebound was driven
29 by increased brine rejection from sea ice formation, triggered by the nearly equal effects of
30 local anomalous winds and surface heat flux. The local divergent wind anomalies promoted
31 local sea ice formation by creating a thin ice area, while a cooling heat flux anomaly
32 decreased the surface temperature, increasing sea ice production. This highlights the
33 importance of understanding local climate variability in projecting future dense shelf water
34 change.

35

36

37

38

39

40

41

42

43

44

45 **Introduction**

46 The Ross Sea provides the densest Dense Shelf Water (DSW, the precursor for Antarctic
47 bottom water (AABW), Figure 1a) on its continental shelf and contributes approximately
48 25% of all AABW formation on the Antarctic shelf (Orsi et al., 2002). Water in the western
49 Ross Sea shelf is particularly important for AABW formation due to its high salinity,
50 resulting from local salt inputs produced during sea ice formation (Rusciano et al., 2013;
51 Sansiviero et al., 2017; Aulicino et al., 2018), together with remote sources advected toward
52 the western Ross Sea by coastal currents (Assmann & Timmermann, 2005; Jendersie et al.,
53 2018).

54 In the western Ross Sea, sea ice is driven northward by the persistent, strong southerly
55 katabatic winds. During the austral winter (April- October), this results in vigorous sea ice
56 formation and brine release, which initiates the formation of high-salinity shelf water and
57 determines its properties (Fusco et al., 2009; Rusciano et al., 2013; Morrison et al., 2023).
58 Moreover, the ocean circulation on the Ross Sea continental shelf consists of two main
59 inflows from the east driven by the easterly wind, the Antarctic Coastal Current and Antarctic
60 Slope Current (Smith Jr et al., 2012). Thus, these westward inflows are essential in
61 transporting fresher water from the upstream Amundsen Sea to the Ross Sea (Figure 1a),
62 influencing the long-term variability of DSW salinity in the western Ross Sea (S. Jacobs et
63 al., 2022).

64 Ocean measurements in the western Ross Sea have shown a significant decrease (~ 0.03 psu
65 per dec) in DSW salinity from 1958 to 2008 (Jacobs & Giulivi, 2010), which is thought to be
66 driven by enhanced Antarctic melting in the Amundsen Sea (Nakayama et al., 2014).

67 Beginning in the early 2010s, however, the DSW salinity in the western Ross Sea
68 experienced a sharp rebound, with values in 2018 comparable to those in the mid-late 1990s
69 (Castagno et al., 2019). This salinity rebound contradicts the expectation that the ongoing

70 increased ice-sheet mass loss in West Antarctica would continue to decrease rather than
71 increase DSW salinity in the western Ross Sea (Jacobs & Giulivi, 2010). Silvano et al.
72 (2020), based on in situ observations, linked this salinity recovery to the enhanced sea ice
73 formation driven by weakened easterly winds from the Amundsen Sea. However,
74 insufficient observations limit a more comprehensive analysis of the individual physical
75 interactions among the atmosphere, ocean, and sea ice that influence salinity variations in the
76 western Ross Sea. In this work, we used a well-tuned global ocean sea-ice model and
77 designed perturbation experiments to isolate the response of shelf water salinity to various
78 atmospheric forcing, aiming to unravel the cause of observed salinity rebound. Our study
79 highlights the importance of integrating observational data with model studies.

80 **2 Model and experiment design**

81 *2.1 In situ hydrographic data*

82 The observational data used in this study were sourced from in-situ salinity observations by
83 Castagno et al. (2019), covering the period from 1995 to 2018 with sampling during most
84 summers within this period. Hydrographic measurements in Terra Nova Bay (defined by
85 74.25° – 75.50° S, 163° – 166° E) with station depths deeper than 800 m have been used. The
86 region chosen is representative of DSW conditions in the western Ross Sea with a marked
87 rebound since the early 2010s (Figure 1b, red line). To compare with observations, model
88 results are sampled in the same area for those years in which the observation data were taken
89 (Figure 1b black line).

90 *2.2 Model description*

91 We adopted the Australian Community Climate and Earth System Simulator – Ocean Model
92 2 (ACCESS-OM2) (Kiss et al., 2020) with a configuration of 1-degree horizontal resolution
93 and 50 z^* vertical levels covering from the surface to 5363.5m depth. The atmospheric

94 forcing derived from JRA55-do (Tsujino et al., 2018), including wind speed, air temperature
 95 and humidity, radiation, precipitations, and sea level pressure, are used to diagnose air–sea
 96 fluxes (wind stress, heat flux, and freshwater flux) through bulk formulae and interactive
 97 coupling between ocean and sea ice. Freshwater flux and heat flux are defined as positive
 98 downward (i.e., freshwater/heat gain by the ocean). In this study, ACCESS-OM2 is
 99 initialized from a state of rest, with temperature and salinity fields coming from the World
 100 Ocean Atlas 2013 v2 monthly climatology (WOA13; (Locarnini et al., 2013; Zweng et al.,
 101 2013)).

102 After a 200-year spin-up under repeated 1990-1991 JRA55-do forcing (Tsujino et al., 2018),
 103 the model reached quasi-equilibrium and was then forced with the 3-hourly JRA55-do
 104 interannual year forcing for 29 years from 1 January 1990 to 31 December 2018. Our analysis
 105 focuses on the recent period 2000–2018. In this study, we used annual data from both model
 106 simulations and observations to ensure a consistent comparison between the two of them.
 107 More detailed information on the model setup can be found in the Supporting Information.

108 *2.3 Surface salinity budget analysis*

109 To quantify the processes driving surface salinity anomalies in our simulation, we use the
 110 surface salinity budget terms diagnosed in the model. At the surface, the ocean salinity
 111 budget in a grid cell is given by:

$$112 \quad \frac{\partial S}{\partial t} = -\nabla \cdot (\mathbf{u}S) + \nabla \cdot (K_{eddy}S) + \nabla \cdot (K_{small}S) + \frac{(E-P-R)S}{h} + \frac{\rho_l I(S-S_l)}{\rho_0 h} \quad (1)$$

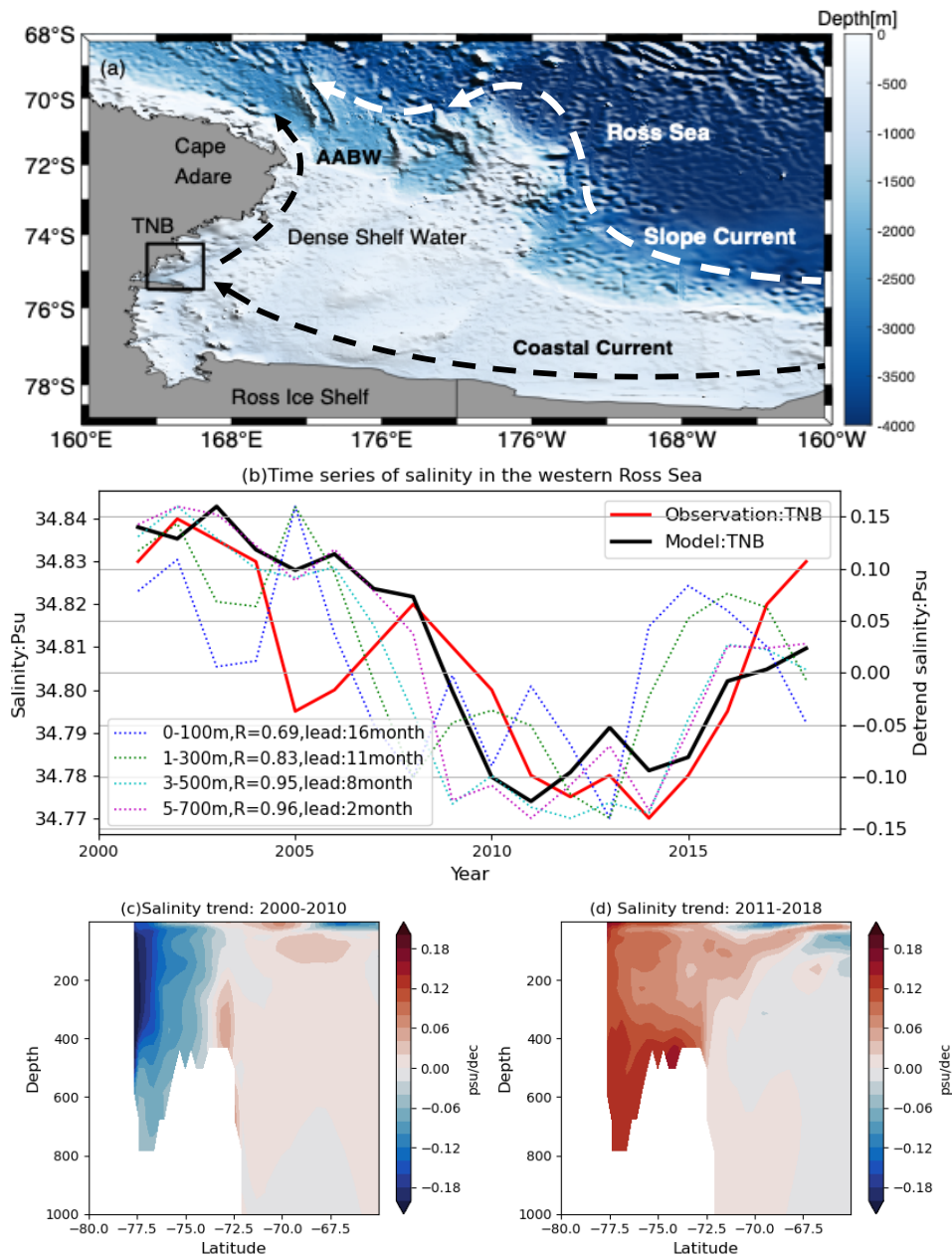
113 where S is sea surface salinity, $\partial S/\partial t$ is the salinity tendency, h is the grid cell thickness, and
 114 \mathbf{u} is the three-dimension velocity. K_{eddy} is the diffusion tensor for mesoscale mixing, and
 115 K_{small} represents vertical diffusion and other mixing processes smaller than eddies. E and P
 116 are the rates of evaporation and precipitation (positive upward), and R is river runoff and

117 meltwater from Antarctica and Greenland. I is the rate of sea ice formation while S_I is sea ice
118 salinity. ρ_o and ρ_I are the reference seawater density and sea ice density, respectively.
119 In ACCESS-OM2 model, ocean salt content is conserved in each grid cell within the
120 expected numerical precision. The salinity budget in Eq. 1 states that the time tendency of
121 salinity (left-hand side) equals all contributing terms (right-hand side), including salt
122 convergences due to the oceanic processes (advection, the first term, and diffusion, the
123 second and third term), evaporation minus precipitation, runoff and meltwater, and sea ice.
124 We use these salinity budget terms to isolate the respective contributions of these processes to
125 the salinity rebound in our perturbation experiment.

126 *2.4 Experiment design*

127 In this study, we designed three perturbation experiments to investigate the role of
128 atmospheric forcing in the rebound of shelf water salinity in the western Ross Sea (Table in
129 the Supporting Information). In the first experiment, the All-Vary experiment, the ACCESS-
130 OM2 model is forced with prescribed atmospheric conditions taken from the JRA55-do 3-
131 hourly forcing from 2010 to 2018. In the second experiment from 2010 to 2018, the Wind-
132 Vary experiment, the wind forcing is the same as in the All-Vary experiment, and the rest of
133 the atmospheric forcing is replaced by the 3-hourly climatological forcing (derived over the
134 2000-2010 base period). In the third experiment from 2010 to 2018, the All-Fixed
135 experiment, all the atmospheric forcing is replaced by the climatological forcing (derived
136 over the 2000-2010 base period). In ACCESS-OM2, the ocean and sea ice models are forced
137 by the surface heat flux, freshwater flux, and wind stress calculated on-the-fly from
138 prescribed atmospheric conditions and model states. The ongoing increased Antarctic
139 meltwater is not expected to explain the observed rapid salinity rebound (Adusumilli et al.,
140 2020). Other freshwater flux, including precipitation, evaporation, and runoff, has a minimal
141 impact on the salinity in the western Ross Sea (Jacobs & Giulivi, 2010; Porter et al., 2019).

142 Therefore, changes in atmospheric forcing in the study region, are mainly from surface heat
 143 flux and wind stress. We then compared the Wind-Vary experiment versus the All-Fixed
 144 experiment to isolate the impact of wind stress and compared the All-Vary experiment versus
 145 the Wind-Vary experiment to isolate the shelf water salinity response to surface heat flux
 146 anomaly.



147

148 **Figure 1 | Recent Recovery of DSW salinity in the Western Ross Sea.** (a) Map of the
 149 Ross Sea and the study area in Terra Nova Bay (TNB, solid box). Bottom topography (m) is
 150 shown in color (Amante & Eakins, 2009). White and black dashed lines represent the general

151 currents along the shelf break and on the shelf, referred to Smith et al. (2014). **(b)** Time series
152 of averaged DSW salinity measured (solid red line) and simulated (solid black line) near the
153 seafloor, as well as detrended model simulations at different depth ranges from surface to 700
154 m (dashed lines) and their leading correlations with salinity near the seafloor. Simulated
155 zonal-averaged salinity trends from 2000-2010 **(c)** and 2011-2018 **(d)**.

156

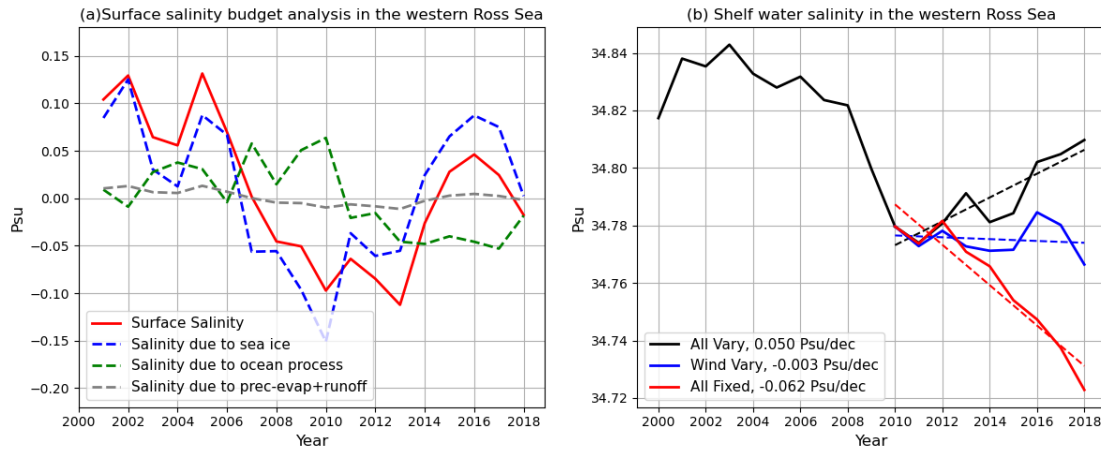
157 **3. Results**

158 *3.1 Observed salinity variations in the western Ross Sea reproduced by model simulations*

159 Figure 1 shows the map of the study area, and the observed and modelled salinities over
160 different depth ranges in the western Ross Sea. The decreasing trend of DSW salinity near the
161 seafloor before the early 2010s is estimated to be -0.05 psu/dec (Figure 1b, red line), slightly
162 larger than the long-term trend of -0.03-0.04 psu/dec estimated by Jacobs et al. (2002) and
163 Jacobs and Giulivi (2010). However, after reaching a minimum in the early 2010s, the
164 freshening trend appears to reverse with a rapid salinity rebound (Figure 1b, red line). The
165 DSW salinity in Terra Nova Bay (TNB) had rebounded up to 2018, reaching its value in the
166 mid-late 1990s, indicating a recent recovery of DSW salinity in the western Ross Sea
167 (Castagno et al., 2019). The observed decrease of DSW salinities between 2000 and the early
168 2010s followed by the sharp rebound is reproduced well by our model simulation based on
169 ACCESS-OM2 (Figure 1b, red and black lines).

170 This recent sharp salinity rebound is simulated throughout the entire water column from
171 surface to the bottom (Figures 1b, 1c, 1d, and Figure S1 in Supporting Information),
172 supported by a strong correlation, with surface salinity leading seafloor salinity at a
173 maximum of 16 months ($r = 0.69$, $p < 0.05$). We then discuss the drivers of the recent DSW
174 salinity rebound since the early 2010s based on our model simulation.

175



176 **Figure 2 | Recent Recovery of DSW salinity induced by atmospheric forcing.** (a) Time
 177 series of detrended model simulated surface salinity (red line) in western Ross Sea (162°E-
 178 168°E, 74°S-78°S), and time integrated surface salinity changes due to sea ice (blue line), net
 179 precipitation plus runoff (grey line) and oceanic process (green line) from 2000 to 2018. (b)
 180 Time series of averaged DSW salinity simulated by All Vary (black line) from 2000 to 2018,
 181 Wind Vary (blue line) and All Fixed (red line) and their trends (dashed lines) from 2011 to
 182 2018 near the seafloor in TNB. Trend values are given in the legend in PSU per decade.

183

184 *3.2 The effects of atmospheric forcing on recent salinity rebound through sea ice formation*

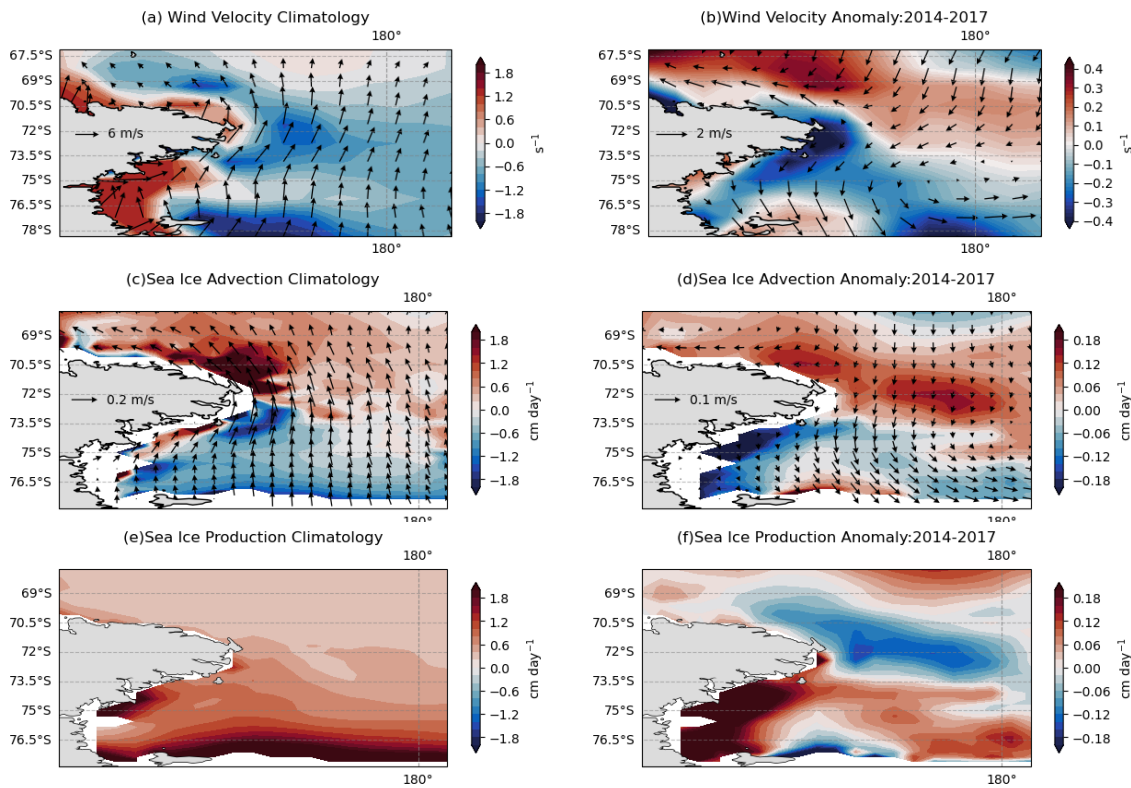
185 A surface salinity budget analysis based on our model simulation (Figure 2a) reveals that
 186 increased brine rejection from sea ice production largely drives the recent salinity rebound
 187 over the western Ross Sea between 2010 and 2018. Oceanic processes counteract the salinity
 188 tendency implied by sea ice brine rejection. Other freshwater sources, such as precipitation
 189 minus evaporation, runoff, and Antarctic meltwater, exert minimal impact and cannot explain
 190 the observed rapid DSW salinity rebound. This is substantiated by hydrographic
 191 measurements that neither support a reduced net precipitation over the Ross Sea continental
 192 shelf (Porter et al., 2019) nor evidence of a decline in freshwater inflow from the Amundsen
 193 Sea (Adusumilli et al., 2020).

194 To further determine which atmospheric forcing is responsible for the recent salinity rebound,
195 we conduct three perturbation experiments: All-Fixed, Wind-Vary, and All-Vary (see Table
196 in Supporting Information). In the All-Fixed experiment, with atmospheric forcing remaining
197 fixed to its climatology from 2000 to 2010, a negative trend in the salinity of the DSW is
198 simulated (-0.062 psu/dec from 2011 to 2018, red line in Figure 2b), which is roughly
199 consistent with the declining trend observed from the 1990s to the early 2010s (Jacobs &
200 Giulivi, 2010; Castagno et al., 2019). The All-Fixed experiment suggests that a continued
201 decrease in DSW salinity would be expected in the absence of changes in atmospheric
202 conditions. The Wind-Vary experiment suggests that incorporating real-time wind forcing
203 could basically stop the gradual decrease trend in salinity observed previously over 2000-
204 2010 and stabilize without any obvious trends over 2010-2018 (blue line in Figure 2b). It is
205 important to note that besides wind stress, other atmospheric factors also play a role in sea ice
206 formation. Sea ice formation is closely connected to surface air temperature and sea surface
207 temperature, which, in turn, is influenced by various types of surface heat flux from the
208 atmosphere (Turner et al., 2015; Alekseev et al., 2022).

209 The All-Vary experiments provide compelling evidence that including all the real-time
210 atmospheric forcing results in a notable rebound in DSW salinity in the western Ross Sea of
211 $+0.050$ psu/dec over 2010- 2018, close to observations (Figure 2b, black line). Therefore, our
212 model experiments suggest that the dynamic effect (sea ice formation driven by wind stress
213 anomaly) and thermodynamic effect (sea ice formation driven by surface heat flux anomaly)
214 have comparable impacts on the recent rebound in DSW salinity, contributing ~ 0.050
215 psu/dec each to the rebound (Figure 2b).

216 We next show the processes and mechanisms that how wind forcing (as revealed by
217 comparing Wind-Vary and All-Fixed experiments) and surface heat flux (as revealed by

218 comparing All-Vary and Wind-Vary experiments) cause increased sea ice production that
 219 further induces the recent rebound of DSW salinity in the western Ross Sea.



220 **Figure 3 | Increased sea ice production due to sea ice divergence induced by wind**
 221 **anomalies.** Climatology and 2014-2017 anomalies of winds (**a,b**, vectors, with colour
 222 shading represents wind divergence; negative values denote divergent), sea ice advection [
 223 $\nabla \cdot \mathbf{u}h$] (**c,d**, sea ice motion and sea ice mass advection), and sea ice production (**e,f**) induced
 224 by wind forcing.

225

226 3.3 Increased sea ice formation driven by anomalous wind forcing

227 Sea ice dynamical processes, such as a changed sea ice motion in response to changing
 228 surface wind stress, play an important role in the redistribution of sea ice (Holland & Kwok,
 229 2012; Turner et al., 2015). Ice motion is described by ice velocity, whereas sea ice advection
 230 is described here by sea ice convergence [$-\nabla \cdot (\mathbf{u}h)$] (Figures 3c and 3d), where \mathbf{u} is sea ice
 231 velocity and h is sea ice thickness (Zhang et al., 2010). Thus, changes in ice thickness (mass

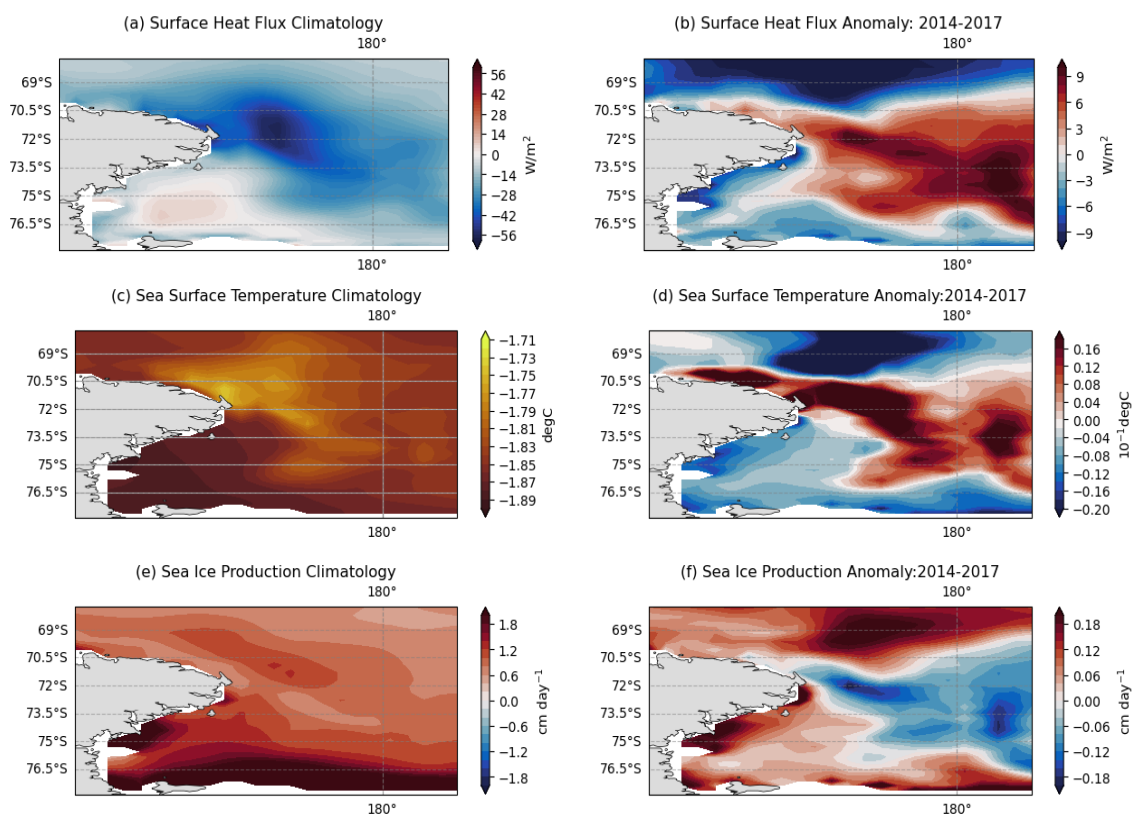
232 gain or loss) due to ice advection quantitatively describe the impact of wind-driven ice
233 motion on sea ice spatial redistribution.

234 Mass loss due to sea ice advection generally occurs in the south region of the western Ross
235 Sea, and ice gain occurs in the north (Figure 3c), indicating a sea ice motion from south to
236 north in the Western Ross Sea (Comiso et al., 2011; Holland & Kwok, 2012; Turner et al.,
237 2015). Such a sea ice advection pattern is attributed to strong northward ice motion driven by
238 the coastal currents and strong southerly winds prevailing in winter (Holland & Kwok, 2012;
239 Turner et al., 2016). During the period of 2014-2017, however, a local wind stress anomaly in
240 the western Ross Sea displayed a divergent pattern (Figure 3b, blue shading). This anomaly
241 had a notable impact on the motion of sea ice, particularly in impeding its northward motion,
242 resulting in ice loss in the western Ross Sea (Figure 3d, blue shading, change in ocean
243 circulation is negligible in our Wind-Vary experiment) and concurrent ice gain in the Ross
244 Sea polynya near the coast (Figure 3d, red shading). Consequently, local changes in ice
245 thickness (gain and loss) due to this reduced northward ice transport can be up to 0.2 cm/day,
246 leading to the expansion of a larger area of thin ice in the north and a narrow area of thick ice
247 near the coast (Figure S4). This increased presence of thin ice contributes to enhanced ice
248 growth and brine rejection (Figure 3f), as growth rates of thin ice are higher compared to
249 thick ice (Zhang et al., 2010).

250 The significant negative spatial correlation between the simulated anomalies of sea ice
251 advection and sea ice production (Figures 3d, 3f, $r = -0.73$, $p < 0.01$) further highlights the
252 close relationship between wind-driven sea ice mass advection and ice production.

253 Additionally, the sea ice loss (gain) resulting from sea ice mass advection exhibits a
254 significant correlation with the wind divergence anomaly over the western Ross Sea (Figures
255 3b and 3d, $r = 0.67$, $p < 0.01$). These findings suggest that, in the Wind-Vary experiment, wind
256 forcing plays a dominant role in the formation of ice in the Ross Sea, primarily through ice

257 mass advection processes. To identify the region where the wind forcing is responsible for
 258 the changes in sea ice in the Western Ross Sea, we conducted further experiments
 259 (Supporting Information 1.4 and Figure S2). Our investigation reveals that only when
 260 applying real-time wind forcing in the western Ross Sea region (160°E-170°W, 60°S-80°S)
 261 the model is able to successfully simulate the increased salinity of DSW driven by wind
 262 (Figures S2 and S3). This suggests that the wind-driven component of the simulated increase
 263 in DSW salinity is primarily driven by local wind anomalies rather than non-local wind
 264 originating from distant regions. Thus, during the period of 2014-2017, the amplified sea ice
 265 production and brine rejection observed in the Wind-Vary experiment in the western Ross
 266 Sea can be attributed to the thinning of sea ice caused by local divergent wind anomalies.



267 **Figure 4 | Increased sea ice production due to lower temperatures induced by surface**
 268 **heat flux anomalies.** Climatology and 2014-2017 anomalies of surface heat flux (Wm^{-2} ;
 269 positive downward) (a,b), sea surface temperature ($^{\circ}C$) (c,d) and sea ice production (cm/day)
 270 (e,f) induced by atmospheric forcing other than wind.

271 3.4 Increased sea ice formation driven by surface heat flux

272 In addition to the dynamical processes induced by wind, thermodynamic processes can also
273 play an important role in the production of sea ice. During the sea ice growth season, the
274 surface heat flux plays a crucial role in influencing sea ice production by affecting the sea
275 surface temperature (Turner et al., 2015; Alekseev et al., 2022). During the period of 2014-
276 2017, a comparison between All-vary and wind-vary model experiments reveals that with a
277 decrease in surface heat flux from the atmosphere, there is a corresponding decrease in upper-
278 ocean temperature (Figures 4b and 4d) in the western Ross Sea. This decrease in temperature
279 promotes an increase in sea ice growth, resulting in increased brine rejection from the new ice
280 and subsequently contributing to an increased salinity from surface to seafloor in the western
281 Ross Sea (Figures 2b and 4f). The significant spatial correlation between the anomalies of
282 surface heat flux and sea surface temperature (Figures 4b and 4d, $r = 0.68$, $p < 0.01$), and sea
283 ice production (Figures 4b and 4f, $r = 0.63$, $p < 0.01$) further highlights the strong connection
284 between surface heat flux and sea ice production.

285 It is essential to note that contrary to a simplistic inverse correlation, the relationship between
286 sea surface temperature and net sea ice production is more intricate (Zhang, 2007). Our
287 simulations indicate that in the upper 200 meters of the western Ross Sea, an increase in
288 salinity and a decrease in temperature lead to increased ocean density (Figure S5). This
289 increased upper-ocean density in turn reduces stratification (the denser layer above the lighter
290 layer) and enhances vertical heat exchange, leading to a greater upward ocean heat transport
291 available to melt the sea ice (Zhang, 2007; Turner et al., 2015). The pivotal balance of sea ice
292 thus lies between the initial sea ice growth driven by surface cooling and the sea ice melt
293 induced by vertical heat flux from the subsurface. In line with this, our model exhibits a
294 positive anomaly in local net ice production of 0.2 cm/day (Figure 4f), primarily driven by a
295 more pronounced increase in ice growth compared to ice melt (Figure S6). Hence, the overall

296 increase in net sea ice production and brine rejection due to the thermodynamic process is
297 driven by the rate of ice growth—induced by lower surface temperatures— surpassing the
298 rate of ice melt, which itself is influenced by increased convective overturning and resultant
299 upward ocean heat transport.

300 **4. Discussion and conclusions**

301 This study presents results from a model study of the recent rebound of DSW salinity in the
302 western Ross Sea. Sea surface salinity budget analysis shows that the recent salinity rebound
303 is dominated by increased brine rejection from sea ice formation, which further propagates
304 and extends the whole water column from surface to seafloor (0-900 m). We further conduct
305 three model perturbation experiments and find that this increased sea ice formation is driven
306 by the combined effect of anomalous local wind stress and surface heat flux, which have
307 nearly equal impacts on shelf water salinity rebound through dynamic and thermodynamic
308 processes. During 2014-2017, the local wind anomalies induced a divergent motion in sea
309 ice, reducing sea ice thickness and promoting local sea ice formation. Meanwhile, cooling
310 heat flux anomaly from the atmosphere cools the surface, increasing sea ice production in
311 winter.

312 The Southern Oscillation Index (SOI) captures variability associated with the ENSO events,
313 influencing the low-pressure system over the Amundsen Sea (Amundsen Sea Low, ASL)
314 through the atmospheric teleconnection (Lee & Jin, 2023). A negative SOI (corresponding to
315 an El Niño event) over 2014-2017 (Figure S7a) influenced an eastward and northward shift of
316 the ASL central (Figure S7b) (Raphael et al., 2016), leading to a reduction in the meridional
317 sea level pressure gradient in the western Ross Sea (Figures S7 c,d) (Coggins & McDonald,
318 2015), thus weakening southerlies and reducing surface heat flux in the western boundary
319 (Clem et al., 2017), ultimately leading to the recent rebound of DSW salinity through sea ice
320 formation.

321 Long-term observations have recorded a freshening AABW over the past 60 years (Jacobs &
322 Giulivi, 2010; Silvano et al., 2018), as a result of increased Antarctic meltwater (Lago &
323 England, 2019; Johnson, 2022). Our study reveals that climate variability can temporally
324 counteract this long-term freshening by enhancing sea ice formation and brine rejection.
325 Future climate projections show an increased frequency of extreme El Niño events due to the
326 greenhouse warming (Cai et al., 2014), therefore possibly enhancing AABW formation that
327 potentially offsets or even surpasses the meltwater-induced freshening on different time
328 scales. Thus, the experiment design and salinity budget analysis conducted here provide an
329 essential reference for identifying the major drivers of the shelf water salinity variations from
330 interannual to decadal time scales.

331

332 **Acknowledgments**

333 This research was supported by the Australian Research Council Special Research Initiative,
334 the Australian Centre for Excellence in Antarctic Science (Project Number SR200100008),
335 and the Centre for Southern Hemisphere Oceans Research (CSHOR), jointly funded by the
336 Commonwealth Scientific and Industrial Research Organisation (CSIRO, Australia) and the
337 Qingdao National Laboratory for Marine Science and Technology (QNLN, China). This
338 research was undertaken with the assistance of resources from the National Computational
339 Infrastructure (NCI Australia). The authors thank the Consortium for Ocean-Sea Ice
340 Modelling in Australia (COSIMA; <http://www.cosima.org.au>) for making the ACCESS-OM2
341 suite of models available at <https://github.com/COSIMA/access-om2>.

342

343

344

345 **Data Availability Statement**

346 The observational data used in this study were sourced from in-situ salinity observations by
347 Castagno et al. (2019), covering the period from 1995 to 2018. The model source code is
348 available from <https://github.com/COSIMA/access-om2/>. The configuration files for the
349 repeat year forced simulation are available from https://github.com/COSIMA/1deg_jra55_ryf
350 and for the interannually forced simulation from https://github.com/COSIMA/1deg_jra55_iaf
351 Mode experiment and outputs are available from the Zenodo repository at
352 <https://doi.org/10.5281/zenodo.8415955>

353

354 **Reference**

- 355 Adusumilli, S., Fricker, H. A., Medley, B., Padman, L., & Siegfried, M. R. (2020). Interannual
356 variations in meltwater input to the Southern Ocean from Antarctic ice shelves.
357 *Nature Geoscience*, 13(9), 616-620.
- 358 Alekseev, G., Vyazilova, A., & Smirnov, A. (2022). Influence of Sea Surface Temperature in
359 the Tropics on the Antarctic Sea Ice during Global Warming. *Journal of Marine
360 Science and Engineering*, 10(12), 1859.
- 361 Amante, C., & Eakins, B. W. (2009). ETOPO1 arc-minute global relief model: procedures,
362 data sources and analysis.
- 363 Assmann, K. M., & Timmermann, R. (2005). Variability of dense water formation in the Ross
364 Sea. *Ocean Dynamics*, 55(2), 68-87.
- 365 Aulicino, G., Sansiviero, M., Paul, S., Cesarano, C., Fusco, G., Wadhams, P., & Budillon, G.
366 (2018). A new approach for monitoring the Terra Nova Bay polynya through MODIS
367 ice surface temperature imagery and its validation during 2010 and 2011 winter
368 seasons. *Remote Sensing*, 10(3), 366.
- 369 Cai, W., Borlace, S., Lengaigne, M., Van Rensch, P., Collins, M., Vecchi, G., et al. (2014).
370 Increasing frequency of extreme El Niño events due to greenhouse warming. *Nature
371 Climate Change*, 4(2), 111-116.
- 372 Castagno, P., Capozzi, V., DiTullio, G. R., Falco, P., Fusco, G., Rintoul, S. R., et al. (2019).
373 Rebound of shelf water salinity in the Ross Sea. *Nature communications*, 10(1), 1-6.
- 374 Clem, K. R., Renwick, J. A., & McGregor, J. (2017). Large-scale forcing of the Amundsen Sea
375 low and its influence on sea ice and West Antarctic temperature. *Journal of Climate*,
376 30(20), 8405-8424.
- 377 Coggins, J. H., & McDonald, A. J. (2015). The influence of the Amundsen Sea Low on the
378 winds in the Ross Sea and surroundings: Insights from a synoptic climatology. *Journal
379 of Geophysical Research: Atmospheres*, 120(6), 2167-2189.

380 Comiso, J. C., Kwok, R., Martin, S., & Gordon, A. L. (2011). Variability and trends in sea ice
381 extent and ice production in the Ross Sea. *Journal of Geophysical Research: Oceans*,
382 116(C4).

383 Fusco, G., Budillon, G., & Spezie, G. (2009). Surface heat fluxes and thermohaline variability
384 in the Ross Sea and in Terra Nova Bay polynya. *Continental Shelf Research*, 29(15),
385 1887-1895.

386 Holland, P. R., & Kwok, R. (2012). Wind-driven trends in Antarctic sea-ice drift. *Nature*
387 *Geoscience*, 5(12), 872-875.

388 Jacobs, & Giulivi. (2010). Large multidecadal salinity trends near the Pacific–Antarctic
389 continental margin. *Journal of Climate*, 23(17), 4508-4524.

390 Jacobs, Giulivi, & Mele, P. (2002). Freshening of the Ross Sea during the late 20th century.
391 *Science*, 297(5580), 386-389.

392 Jacobs, S., Giulivi, C., & Dutrieux, P. (2022). Persistent Ross Sea freshening from imbalance
393 West Antarctic ice shelf melting. *Journal of Geophysical Research: Oceans*, 127(3),
394 e2021JC017808.

395 Jendersie, S., Williams, M. J., Langhorne, P. J., & Robertson, R. (2018). The density-driven
396 winter intensification of the Ross Sea circulation. *Journal of Geophysical Research:*
397 *Oceans*, 123(11), 7702-7724.

398 Johnson, G. C. (2022). Antarctic Bottom Water Warming and Circulation Slowdown in the
399 Argentine Basin From Analyses of Deep Argo and Historical Shipboard Temperature
400 Data. *Geophysical Research Letters*, 49(18), e2022GL100526.

401 Kiss, A. E., Hogg, A. M., Hannah, N., Boeira Dias, F., Brassington, G. B., Chamberlain, M. A., et
402 al. (2020). ACCESS-OM2 v1. 0: a global ocean–sea ice model at three resolutions.
403 *Geoscientific Model Development*, 13(2), 401-442.

404 Lago, V., & England, M. H. (2019). Projected slowdown of Antarctic bottom water formation
405 in response to amplified meltwater contributions. *Journal of Climate*, 32(19), 6319-
406 6335.

407 Lee, H.-J., & Jin, E. K. (2023). Understanding the delayed Amundsen Sea low response to
408 ENSO. *Frontiers in Earth Science*, 11, 1136025.

409 Locarnini, R., Mishonov, A., Antonov, J., Boyer, T., Garcia, H., Baranova, O., et al. (2013).
410 World Ocean Atlas 2013, Volume 1: Temperature in: NOAA Atlas NESDIS 73 edited
411 by S. In: Levitus.

412 Morrison, A. K., Huneke, W. G., Neme, J., Spence, P., Hogg, A. M., England, M. H., & Griffies,
413 S. M. (2023). Sensitivity of Antarctic shelf waters and abyssal overturning to local
414 winds. *Journal of Climate*, 1-32.

415 Nakayama, Y., Timmermann, R., Rodehacke, C. B., Schröder, M., & Hellmer, H. H. (2014).
416 Modeling the spreading of glacial meltwater from the Amundsen and Bellingshausen
417 Seas. *Geophysical Research Letters*, 41(22), 7942-7949.

418 Orsi, A. H., Smethie Jr, W. M., & Bullister, J. L. (2002). On the total input of Antarctic waters
419 to the deep ocean: A preliminary estimate from chlorofluorocarbon measurements.
420 *Journal of Geophysical Research: Oceans*, 107(C8), 31-31-31-14.

421 Porter, D. F., Springer, S. R., Padman, L., Fricker, H. A., Tinto, K. J., Riser, S. C., et al. (2019).
422 Evolution of the seasonal surface mixed layer of the Ross Sea, Antarctica, observed
423 with autonomous profiling floats. *Journal of Geophysical Research: Oceans*, 124(7),
424 4934-4953.

425 Raphael, M. N., Marshall, G., Turner, J., Fogt, R., Schneider, D., Dixon, D., et al. (2016). The
426 Amundsen Sea low: Variability, change, and impact on Antarctic climate. *Bulletin of*
427 *the American Meteorological Society*, 97(1), 111-121.

428 Rusciano, E., Budillon, G., Fusco, G., & Spezie, G. (2013). Evidence of atmosphere–sea ice–
429 ocean coupling in the Terra Nova Bay polynya (Ross Sea—Antarctica). *Continental*
430 *Shelf Research*, 61, 112-124.

431 Sansiviero, M., Maqueda, M. M., Fusco, G., Aulicino, G., Flocco, D., & Budillon, G. (2017).
432 Modelling sea ice formation in the Terra Nova Bay polynya. *Journal of Marine*
433 *Systems*, 166, 4-25.

434 Silvano, A., Foppert, A., Rintoul, S. R., Holland, P. R., Tamura, T., Kimura, N., et al. (2020).
435 Recent recovery of Antarctic Bottom Water formation in the Ross Sea driven by
436 climate anomalies. *Nature Geoscience*, 13(12), 780-786.

437 Silvano, A., Rintoul, S. R., Peña-Molino, B., Hobbs, W. R., van Wijk, E., Aoki, S., et al. (2018).
438 Freshening by glacial meltwater enhances melting of ice shelves and reduces
439 formation of Antarctic Bottom Water. *Science Advances*, 4(4), eaap9467.

440 Smith Jr, W. O., Sedwick, P. N., Arrigo, K. R., Ainley, D. G., & Orsi, A. H. (2012). The Ross Sea
441 in a sea of change. *Oceanography*, 25(3), 90-103.

442 Smith, W. O., Dinniman, M. S., Hofmann, E. E., & Klinck, J. M. (2014). The effects of changing
443 winds and temperatures on the oceanography of the Ross Sea in the 21st century.
444 *Geophysical Research Letters*, 41(5), 1624-1631.

445 Tsujino, H., Urakawa, S., Nakano, H., Small, R. J., Kim, W. M., Yeager, S. G., et al. (2018). JRA-
446 55 based surface dataset for driving ocean–sea-ice models (JRA55-do). *Ocean*
447 *Modelling*, 130, 79-139.

448 Turner, J., Hosking, J. S., Bracegirdle, T. J., Marshall, G. J., & Phillips, T. (2015). Recent
449 changes in Antarctic sea ice. *Philosophical Transactions of the Royal Society A:*
450 *Mathematical, Physical and Engineering Sciences*, 373(2045), 20140163.

451 Turner, J., Hosking, J. S., Marshall, G. J., Phillips, T., & Bracegirdle, T. J. (2016). Antarctic sea
452 ice increase consistent with intrinsic variability of the Amundsen Sea Low. *Climate*
453 *Dynamics*, 46, 2391-2402.

454 Zhang, J. (2007). Increasing Antarctic sea ice under warming atmospheric and oceanic
455 conditions. *Journal of Climate*, 20(11), 2515-2529.

456 Zhang, J., Woodgate, R., & Moritz, R. (2010). Sea ice response to atmospheric and oceanic
457 forcing in the Bering Sea. *Journal of Physical Oceanography*, 40(8), 1729-1747.

458 Zweng, M., Reagan, J., Antonov, J., Locarnini, R., Mishonov, A., Boyer, T., et al. (2013). World
459 Ocean atlas 2013. Vol. 2. Salinity. NOAA Atlas NESDIS 74. In: Silver Spring, MD:
460 National Oceanic and Atmospheric Administration, National
461